Talanta 223 (2021) 121739

Contents lists available at ScienceDirect

Talanta

journal homepage: www.elsevier.com/locate/talanta

Rapid vertical flow immunoassay on AuNP plasmonic paper for SERS-based point of need diagnostics

Richard Frimpong, Wongi Jang [1], Jun-Hyun Kim [**], Jeremy D. Driskell [*]

Department of Chemistry, Illinois State University, Normal, IL, 61790, USA

ARTICLE INFO

Keywords:
Immunoassay
Surface-enhanced Raman scattering (SERS)
Plasmonic paper
Vertical flow assay
Point-of-need (PON) testing
Point-of-care (POC) diagnostics°

ABSTRACT

SERS based immunoassays for point-of-care diagnostics are a promising tool to facilitate biomarker detection for early disease diagnosis and disease control. The technique is based on a sandwiched system in which antigen is first captured by a selective plasmonic paper substrate and then labeled by an extrinsic Raman label (ERL), consisting of a 60 nm gold nanoparticle (AuNP) functionalized with a mixed monolayer of detection antibody and 4-nitrobenezenethiol (NBT) as a Raman reporter molecule. Here, we report on the use of AuNP modified filter paper as a novel capture membrane in a vertical flow format. This vertical flow configuration affords reproducible flow of sample and label through the capture substrate to overcome diffusion limited kinetics and significantly reduced assay time. The filter paper was selected due to its affordability and availability, while the embedded AuNPs maximized plasmonic coupling with the ERLs and SERS enhancement. Additionally, the embedded AuNP served as a scaffold to immobilize capture antibody to specifically bind antigen. In this work, a SERS-based rapid vertical flow (SERS-RVF) immunoassay for detection of mouse IgG was developed to establish proof-of-principle. Optimization of assay conditions led to a limit of detection of 3 ng/mL, which is comparable to more traditional formats carried out in multi-well plates, and significantly reduced assay time to less than 2 min. Additionally, IgG was accurately quantified in normal mouse serum to validate the SERS-RVF assay for application to the analysis of biological samples. These results highlight the potential advantages of the SERS-RVF platform for point-of-need testing.

1. Introduction

Point-of-need (PON) tests are essential for early diagnosis of disease and identification of biological threats [1–3]. These assays must be physically and operationally portable to work in many settings including medical offices, in home, or in the field for military and environmental applications [1–3]. In practice, these applications necessitate that the assay is easy to perform, rapid, and cost-effective, while sensitivity, precision, and quantitation are desirable. Currently, the lateral flow assay (LFA) format has found the most success as point-of-need tests because this format provides the requisite qualities of convenience, speed, and low-cost [4]. However, conventional LFAs that rely on colorimetric readout do not provide low detection limits that often translate into a high rate of false negative tests. Moreover, these LFAs are not quantitative and do not allow for multiplexed detection. With these limitations, much effort has been placed on improving readout strategies to improve LFA sensitivities and moderate success has been reported for detection schemes using enzymes [5], chemiluminescence [6], fluorescence [7–9], and surface-enhanced Raman spectroscopy (SERS) [10–12]. Despite efforts to develop advanced readout technologies for LFAs, this format is inherently limited by the hook effect, which complicates quantitative analysis and results in false negative results at high concentrations [13–15].

Recently, rapid vertical flow (RVF) assays have been explored as alternatives to LFAs that circumvent the inherent limitations of LFAs [16–19]. The sequential application and immunoreaction of the sample and label on the capture substrate eliminates the potential for the hook effect and results are immediately available without the need for assay development time. However, RVF assays that rely on visual readout also lack sensitivity and clinical accuracy. Thus, RVF assays must be coupled with emerging detection technologies to fully address the limitations of current PON tests. Of the detection modalities already explored for

* Corresponding author.
** Corresponding author.
E-mail addresses: jkim5@ilstu.edu (J.-H. Kim), jdriske@ilstu.edu (J.D. Driskell).
[1] Current address: Department of Energy Engineering, Dankook University, Cheonan-si, Chungnam 31116, South Korea.

https://doi.org/10.1016/j.talanta.2020.121739
Received 5 August 2020; Received in revised form 22 September 2020; Accepted 4 October 2020
Available online 10 October 2020

LFA-based PON assays, SERS offers potential advantages with respect to sensitivity and multiplexed detection capabilities.

SERS has been extensively explored as a readout technology for immunoassays with great success in achieving high sensitivity [20–24]. Based on these foundational works, SERS has been extended to LFA [10–12], and more recently, RVF formatted assays [25–28]. In these SERS-PON works, conventional protein-binding membranes were employed as the capture substrate and Raman reporter functionalized nanoparticles served as SERS tags to facilitate detection. In an attempt to garner even greater sensitivity, core-shell nanoparticles have been developed to improve SERS enhancement relative to previously utilized spherical AuNPs as the core of the SERS tag [11,12]. However, it is well established that plasmonic coupling between nanoparticles affords the greatest SERS enhancement [29–31]; thus, the use of novel plasmonic particles alone does not realize the full potential of SERS in PON tests. Our group previously developed a gold-plated membrane filter as a capture substrate for use in a SERS-based flow-through immunoassay that supported plasmonic coupling with SERS tags [32]. However, those membrane filters were not amenable to the RVF format in which sample is passed through the filter by capillary action using an absorbent pad and a syringe was required to pass sample/labeling solution through the filter thereby limiting ease of use and suffering from variable flow rates that marginalized precision. More recently our group developed a SERS-based PON test based on antigen-mediated aggregation of nanoparticle SERS tags in solution followed by capture and concentration of the aggregates using a RVF device to take advantage of plasmonic coupling to generate large signal enhancements [33]. However, the aggregation-based strategy required 60 min to perform and suffered from the hook effect.

With the current efforts to develop paper-based plasmonic substrates, there exists an opportunity to significantly improve SERS-based RVF assay. Our group and others have developed cost-effect, robust, and reproducible methods to easily fabricate plasmonic papers that are ideal for incorporating into a SERS RVF assay as the capture substrate. The embedded AuNPs in the filter paper create small gaps with the bound SERS nanoparticle tag that forms a SERS hot spot to significantly enhance the signal produced by the SERS tag compared to the same SERS tag bound to a non-plasmonic support. In our previous work, we used a layered AuNP system to model a SERS RVF configuration and established proof-of-principle for the marked improvement in SERS enhancement provided by the underlying plasmonic support [34]. Moreover, the pore sizes of the filter paper can be selected to optimize flow speed to maximize antibody-antigen binding efficiency and minimize assay time and nanoparticle loading to maximize coupling and SERS enhancement with the binding of SERS tags bound to captured antigen.

Here we explore the use of AuNP embedded filter paper as a capture substrate in a SERS-based RVF assay as a highly sensitive, rapid, and easy to use PON test that affords quantitative accuracy. We established the feasibility of the platform using a model antibody-antigen system, although the general scheme is easily adaptable for the detection of a variety of target antigens using appropriate antibodies. The plasmonic substrate is clearly demonstrated to provide a significant increase in assay sensitivity. After establishing the role of the plasmonic capture substrate, the analytical performance of the optimized assay was assessed based on the detection limit, sensitivity, specificity, and precision. The concentration of IgG in normal mouse serum was accurately quantified using the developed SERS RVF assay to demonstrate potential for the analysis of clinical samples.

2. Experimental

2.1. Reagents and materials

Gold nanoparticles (AuNPs; 60 nm) were purchased from Ted Pella Inc. and used to synthesis extrinsic Raman labels (ERLs). Bovine serum albumin (BSA), 4-nitrobenzenethiol (4-NBT), Tween 20, and mouse IgG (I5381) were purchased from Sigma-Aldrich. Goat anti-mouse IgG polyclonal antibody (ab 7063) was obtained from Abcam. The polyclonal nature of this antibody allowed its use as both the capture and detection antibody. Normal mouse serum was acquired from Santa Cruz Biotechnology. Phosphate buffered saline (PBS; 10 mM, pH 7.4) and sodium borate buffer (50 mM, pH 8.5) were purchased from Thermo Scientific. Whatman filter paper grades 4 and 40 were used to prepare SERS substrate. A vertical flow device (Zoom Blot Plate) and high capacity absorbing pads were purchased from Vitrozm.

2.2. Synthesis of gold nanoparticles (AuNPs)

Gold nanoparticles (AuNPs) were synthesized and subsequently used to prepare plasmonic paper. It should be noted that preparation of plasmonic paper requires a highly concentrated AuNP suspension and that the purchase of highly concentrated AuNPs were cost-prohibitive; thus, concentrated AuNPs were synthesized. Briefly, AuNPs with ~60 nm diameters were synthesized by the modified thermal reduction method [35,36]. This size was selected because previous works have demonstrated that AuNPs with a diameter of ~60 nm provide the greatest SERS enhancement [30,32,37,38]. An aliquot (2.0 mL) of gold (1 wt% $HAuCl_4 \cdot 3H_2O$) solution was diluted to 100 mL with water in a 250 mL Erlenmeyer flask containing a magnetic stirring bar. After vigorously stirring the solution for 15 min, the flask was heated to boiling. Trisodium citrate (1 wt%; 1.5 mL) was quickly added to the boiling solution, which led to the formation of spherical AuNPs. After completing the reaction, the final solution was adjusted to 80 mL in total volume (exhibiting an extinction maximum of ~2.4) and stored at room temperature without further purification prior to use.

2.3. Preparation of plasmonic paper capture substrate

Whatman grade 4 and 40 filter paper with 8 and 25 μm pores sizes, respectively, were selected to prepare the plasmonic paper capture substrate. Synthesized AuNPs were embedded in the two filter papers using a previously developed dipping method [34,39–41]. The papers were first dried at 50 °C in an oven overnight and then immersed in 10 mL of the synthesized AuNP suspension in a plastic petri dishes (60 mm × 15 mm). After soaking for 24 h, the filter papers were removed from the AuNP suspension and completely dried in the oven (~40 °C). The resulting plasmonic paper was then cut into circles with a 3 mm diameter for use in the SERS immunoassay. Unless noted otherwise, 2 μL of 1 mg/mL goat anti-mouse antibody was applied to the 3 mm plasmonic paper substrate and dried in a desiccator for 1.5 h before use [27].

2.4. Preparation of extrinsic Raman labels (ERLs)

Antibody and a Raman reporter molecule were co-adsorbed onto AuNPs to prepare extrinsic Raman labels (ERLs), following a previously reported procedure [33,42]. A 1.0 mL aliquot of 60 nm AuNPs (Ted Pella, Inc.) was added to a microcentrifuge tube and 40 μL of 50 mM borate buffer (pH 8.5) was introduced to adjust the pH. AuNPs were purchased to prepare the ERLs because we previously optimized the functionalization conditions for the commercially available AuNPs. Moreover, the purchased AuNPs are more homogeneous than synthesized AuNPs to improve reproducibility. Goat anti-mouse IgG antibody (30 μg) and 10 μL of 1 mM 4-NBT were added and incubated for 1 h to allow the antibody and 4-NBT to adsorb onto the AuNPs, forming the ERLs. The ERL suspension was centrifuged at 5000 g for 5 min and the supernatant above the pelleted ERLs was discarded to remove excess antibody and 4-NBT that was not adsorbed to the AuNPs. The ERLs were resuspended in 2 mM borate buffer and the centrifugation/resuspension cycle was repeated two additional times. To the purified ERLs, 10 μL of 10% BSA was added to further passivate any remaining surface on the AuNPs and 10 μL of 10% NaCl was added to mimic physiological ionic

strength and prevent protein unfolding.

2.5. Vertical flow immunoassay protocol

Calibration standards of the antigen were prepared by diluting a 1 mg/mL stock solution of mouse IgG to final concentrations of 0.1, 0.5, 1, 10, 50, 100, 200, 300 and 400 ng/mL. Two sets of calibration standards were prepared, one using PBS as the diluent and another using rabbit serum as the diluent. PBS or rabbit serum served as the negative control to assess nonspecific binding and specificity. The capture substrate, comprised of the plasmonic filter paper with pre-adsorbed goat anti-mouse IgG antibody, was then loaded on the adsorbing pad and inserted into a vertical flow device. Once assembled, 1% BSA (100 μL) was added to the sample well, and rapidly passed through the capture substrate into the absorbing pad to block the capture substrate and sample well surface in an effort to prevent nonspecific binding. The sample solution, e.g., calibration standard or normal mouse serum, was then added to the sample well and antigen molecules were captured on the plasmonic paper by the immobilized antibody as the solution freely passed through the capture substrate. Next, ERLs were added to the sample well and passed through the capture substrate to label any captured antigen, with excess ERLs drawn into the absorbing pad. Excess ERLs were removed from the surface of the plasmonic paper by passing a PBS rinse solution containing 5% Tween 20 through the paper. The plasmonic paper was removed and allowed to dry in a desiccator before SERS analysis.

2.6. Instrumentation

The plasmonic papers were examined using FEI-Quanta 450 SEM operating at 20 kV to produced visual images of the papers. Prior to this analysis, the papers were coated with a thin gold film using a Denton vacuum sputter coater (DESK II), to avoid common charging problems. The images were collected to measure the general size distribution of plasmonic particles and to visualize overall packing patterns of the NPs on the surface of the filter paper.

To evaluate SERS response of the vertical flow assay, SERS spectra were collected using an Enwave Optronics, Inc. ProRaman-L-785B instrument configured with a 785 nm excitation source set to 10 mW at the sample surface and a high-sensitivity CCD thermoelectrically cooled to −60 °C. The sample was placed on an x-y-z sample stage and the laser was focused on the substrate surface by maximizing the SERS intensity. After focusing the sample stage was automated to move linearly along the x-direction during the 10-s spectral acquisition as a means of increasing the sampling area on the capture substrate, effectively averaging signal from different locations on the substrate [43]. Five spectra were collected from each sample substrate and baseline corrected using the auto-baseline-2 algorithm built into the Enwave application software (ProRaman Reader V8.2.8).

The adsorption of the antibodies on the AuNPs of the ERL were confirmed by measuring the mean hydrodynamic diameter and polydispersity of the AuNPs before and after the preparation of the ERLs with a Malvern Zetasizer Nano ZSP. Unconjugated AuNP and synthesized ERLS were diluted 2-fold with nano pure water and placed in a microvolume disposable Eppendorf cuvette for DLS analysis. The sample was equilibrated for 60 s prior to analysis and each size measurement was determined from 10 runs, 10 s each.

Synthesized gold nanoparticles used to prepare the plasmonic paper were investigated to assess the number of AuNPs loaded on the filter paper by measuring the extinction of the AuNP suspension before and after adsorption onto the filter paper. The UV–visible instrument used for this analysis was Agilent 8453 spectrophotometer (Agilent Technologies, Santa Clara, CA). The instrument has photodiode detector with a spectral range of 190–1100 nm. Prior to sample analysis the instrument was blanked with 2 mM borate buffer (pH 8.5). The prepared plasmonic paper was also characterized using a surface UV–Vis-IR spectrophotometer (300–1700 nm) equipped with a reflectance probe (StellarNet).

3. Results and discussion

3.1. Assay design and sensing principle

A general overview of the SERS-based vertical flow immunoassay is illustrated in Fig. 1. Central to this platform is AuNP-loaded plasmonic paper, which serves as a capture substrate for the detection of antigens. Antibody is pre-immobilized onto the plasmonic paper and antigen is extracted and concentrated on the substrate as the sample solution passes through to an absorbing pad via capillary action. In a second step, ERLs are spontaneously and vertically passed through the plasmonic paper to specifically label captured antigen and facilitate SERS-based detection. The micron-sized pores in the filter paper allow any excess nanometer-sized ERLs to rapidly and freely pass through the plasmonic paper to waste collected in the absorbent pad. The plasmonic paper provides two key features. First, antibody irreversibly adsorbs onto AuNPs embedded in the filter paper [44–47], to form a robust capture substrate that resists desorption and loss of function while solutions flow through the paper. Recent works have found that native cysteine residues in the antibodies are responsible for protein immobilization on the AuNPs with high affinity [48,49]. Second, the AuNP embedded in the paper will form a sandwich-like structure with ERLs bound to captured antigen. This architecture greatly supports plasmonic coupling between the AuNPs to generate a large localized electric field between the sandwiched nanoparticles and significantly enhance the SERS signal relative to the isolated ERL in the absence of plasmonic coupling [30,34,38,50,51]. In addition to the uniquely designed plasmonic paper to maximize analytical signal, the vertical flow format overcomes diffusional mass transport limitations of traditional immunoassays to substantially reduce assay time and does not suffer from the hook effect, as is the case for lateral flow assays, to improve quantitative capabilities [13–15,52,53].

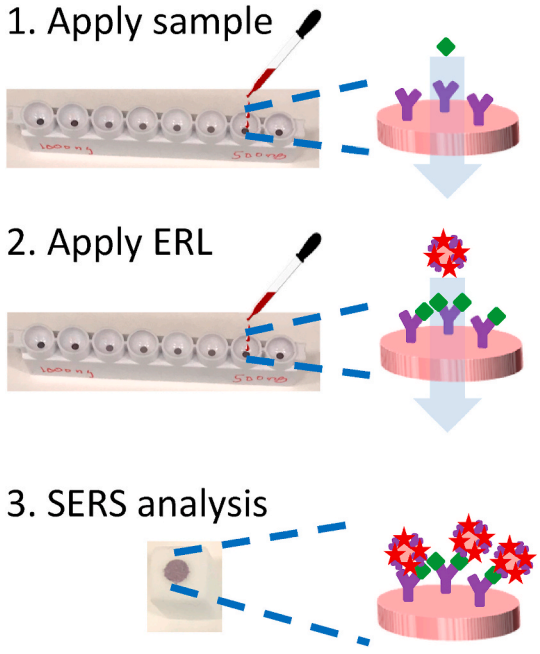

Fig. 1. Illustration of vertical flow immunoassay protocol. In the first step, the sample solution is vertically passed through the paper for antibody to extract the analyte. In the second step, ERLs are passed through paper to label the captured antigen. Photograph of the assembled vertical flow device and the disassembled apparatus with a capture substrate placed on the absorption pad for SERS analysis.

A model antibody-antigen system was employed to establish proof-of-principle for the SERS-based LFA and illustrate the role of the plasmonic capture substrate. The plasmonic capture substrate and ERLs were both synthesized with goat anti-mouse IgG polyclonal antibody and mouse IgG was employed as the antigen. The following sections detail the synthesis of the plasmonic paper, the role of the plasmonic paper to facilitate large SERS enhancements, and the assay parameters that impact analytical performance. After optimization, we defined the analytical figures of merit and applied the protocol to accurately quantify IgG in normal mouse serum.

3.2. Fabrication and characterization of plasmonic paper

Filter paper loaded with spherical AuNPs serve as the foundation of the capture substrate in the SERS-based vertical flow assay illustrated in Fig. 1. Filter paper was selected because of its numerous advantages such as affordability, accessibility, biodegradability, disposability, modification, and variety of unique pore sizes. In this work, we selected Grade 4 and 40 Whatman filter paper with nominal pore sizes of 25 μm and 8 μm, respectively. Fig. 2 shows digital photographs of the two filter papers before and after loading with AuNPs, prepared by dip coating [34, 39–41]. The change in color of the filter paper from white to purple indicates the adsorption of the AuNPs on the paper, and the consistent color across the full paper suggests uniform distribution on a macroscopic scale. SEM images confirm adsorption of the AuNPs onto the fibers of the filter paper with a mean diameter of 57.9 ± 12.5 nm. The images further reveal small aggregates consisting of a few AuNPs are formed on the filter paper during the dip coating process. Moreover, the SEM images show a greater loading density of AuNPs on the grade 4 filter paper than the grade 40 filter paper. The AuNP adsorption efficiency was quantified by the changes of AuNP surface plasmon resonance (SPR) using UV–visible spectrophotometry. The AuNP suspension exhibited an extinction of 2.4 at 540 nm before filter paper was dipped into the suspension. After immersing the filter paper in the AuNP suspension for 24 h and subsequent removal, the remaining suspension displayed an extinction of 0.7 and 1.3 for the grade 4 and 40 filter papers, respectively (Fig. 2). These decreases in SPR bands represent the loading of 2.8×10^{11} AuNPs and 1.8×10^{11} AuNPs on the grade 4 and 40 filter papers, respectively. To support the detectably different amounts of plasmonic AuNP loading onto these two papers, the surface UV–Vis-IR absorption patterns were obtained (Figure S1). Although obtaining surface absorption patterns by a reflectance probe is somewhat difficult due to the light absorbing characteristics of materials, the clearly different SPR patterns (i.e., broader SPR band at 545 nm and increased background peak over 700 nm) explained that the grade 4 filter paper possessed a relatively higher number of locally aggregated AuNPs than the grade 40 filter paper. The presence of slightly more and dense packing of AuNPs could induce a higher probability of effective plasmonic coupling that can favorably influence the degree of SERS enhancements.

3.3. Role of plasmonic paper

SERS-based vertical and lateral flow immunoassays have been previously developed using paper and nitrocellulose membranes as capture substrates. The goal of this work is to capitalize on the benefit afforded by a plasmonic capture substrate to create sandwich-like structures and achieve greater signal enhancements. To establish the value of the plasmonic capture substrate, the RVF assay was performed using unmodified filter paper and plasmonic filter paper. Antibody was deposited on unmodified filter paper and AuNP-embedded filter paper to form the capture substrate [54,55]. After blocking the paper with BSA, 100 μL of the positive control sample (100 ng/mL of mouse IgG) was passed through the capture substrate. The sample solution quickly passed through the unmodified filter paper and grade 4 plasmonic paper in less than 10 s; however, the 100 μL sample required more than 2 min to flow through the grade 40 plasmonic paper. After allowing the sample to completely pass through the capture substrate to the absorbent pad, 100 μL of ERLs were precisely applied to the sample and allowed to pass through the capture substrate to label the antigen extracted by the capture substrate. Again, the ERL flow rate was significantly faster through the grade 4 plasmonic paper than the grade 40 plasmonic paper. After rinsing the paper with PBS (100 μL), SERS spectra were collected to quantify the bound antigen. Representative SERS spectra are presented for each of the capture substrates in Fig. 3. As is evident, the SERS signal is characteristic of the Raman reporter molecule, 4-NBT, used to synthesize the ERLs, and include prominent bands at 1338 cm^{-1} (symmetric NO_2 stretch), 1559 cm^{-1} (C═C), 1153 cm^{-1} (C–O), and 850 cm^{-1} (C–H) [56,57]. Importantly, the signal is markedly increased for the plasmonic paper capture substrates relative to the capture substrate prepared with unmodified filter paper (Fig. 3). Plasmonic paper resulted in ~4-fold and ~10-fold increase in signal for the capture substrate prepared with grade 40 and grade 4 filter paper, respectively, relative to the unmodified paper.

Negative control samples were also analyzed to confirm that the signals obtained for the mouse IgG sample was due to specific antibody-antigen interactions rather than non-specific binding of the ERLs (e.g., physical adsorption) in the filter paper used as the foundation of the capture substrate. To this end, PBS was passed through the capture substrates in the first step. Subsequently, ERLs were passed through the

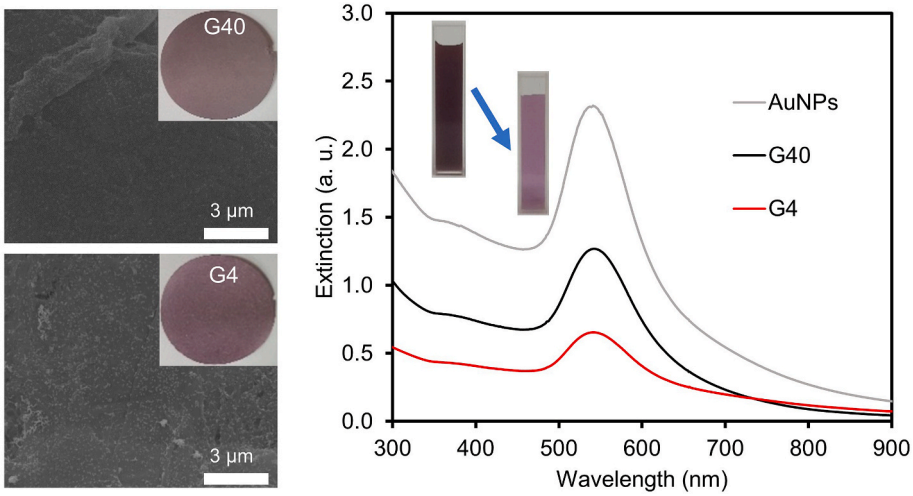

Fig. 2. SEM images of filter paper grade number 4 and 40 with their corresponding UV analysis of AuNPs solution before and after loading on the papers.

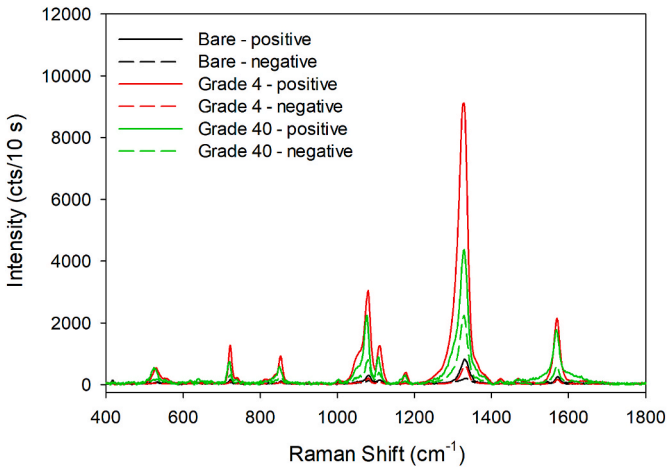

Fig. 3. SERS spectra collected using bare filter paper, plasmonic filter paper grade 4, and plasmonic filter paper grade 40 as the capture substrate in a SERS-RVF immunoassay. The positive control samples represent the analysis of 100 ng/mL mouse IgG and the negative control samples represent the analysis of PBS.

capture substrates and analyzed via SERS (Fig. 3). The signal measured for the PBS negative control was substantially lower than that observed for the analysis of the positive control sample for each of the capture substrates. These results confirm the specificity of antibody-antigen interaction yet reveal some non-specific binding of the ERLs.

Collectively, these results clearly demonstrate greater SERS signals are obtained for the plasmonic capture substrates than the unmodified capture substrate. Interestingly, the plasmonic paper fabricated with grade 4 filter paper provided greater signal for the analysis of the positive control and lower signal for the analysis of the negative control sample than the grade 40 filter paper. As indicated earlier, the SERS enhancement is as a result of interparticle coupling that generates strong localized electromagnetic fields to maximize SERS signal from the substrate. Our results suggest that SERS enhancement provided by the plasmonic capture substrate corresponds to the number of plasmonic nanoparticles that are present on the surface of the paper. Moreover, the paper with the bigger pore size, e.g., grade 4, resulted in less non-specific binding of ERLs to generate less false-positive signal. Owing to this dual benefit, Whatman filter paper grade 4 was selected to prepare plasmonic capture substrates and optimize the assay parameters.

3.4. Assay optimization

3.4.1. Amount of capture antibody

The ability to capture and concentrate antigen on the surface of the plasmonic paper as it passes through correlates with the number of capture antibodies available on the substrate. Therefore, the amount of the antibody deposited on the surface of the paper is an important parameter that can contribute to the analytical performance of the RVF immunoassay. Ideally, sufficient antibody is added to the plasmonic paper to saturate all available immobilization sites. However, addition of a large excess of antibody must be avoided to minimize the cost of the assay. To this end, goat anti-mouse IgG antibody (1–4 μg) was deposited on plasmonic paper (grade 4) to prepare capture substrates with variable amounts of capture antibody. A positive control sample (100 ng/mL antigen) and negative control sample (PBS) were analyzed with each capture substrate, using 100 μL of ERLs and 100 μL of PBS for subsequent labeling and rinsing, respectively. The SERS signal as a function of the amount of capture antibody is plotted for the positive and negative control samples in Fig. 4A. The positive control signal increased as the amount of deposited capture antibody increased from 1 to 2 μg; however, no further increase was observed for the positive control sample with the deposition of more than 2 μg of capture antibody. The signal for the negative control sample was independent of the mass of capture antibody immobilized on the capture substrate. Based on the results of this experiment, 2 μg of capture antibody was selected for cost effectiveness, since this mass provided enough antibodies to effectively maximize the capture of antigen in a 100 ng/mL sample and produce a maximum SERS signal.

3.4.2. Volume of extrinsic Raman labels (ERLs)

The effect of ERL volume on SERS intensity was investigated in an effort to maximize the analytical signal by ensuring all the captured antigen was labeled. Plasmonic paper was loaded with 2 μg of capture antibody to prepare the capture substrate. A positive control sample (100 ng/mL antigen) or a negative control sample (PBS) was passed through the capture substrate followed by varying volumes of ERLs (25, 50, 100, and 200 μL) to label the capture antigens. After rinsing with 100 μL of buffer SERS spectra were collected, and the average intensities are plotted as a function of ERL volume in Fig. 4B. The SERS signal increases as the ERL volume increases from 25 to 100 μL, suggesting that <100 μL of ERLs is insufficient to label all of the captured antigen for a sample concentration of 100 ng/mL. While there was a slight increase in the mean signal when the ERL volume increased from 100 to 200 μL the difference was not statistically different at the 95% confidence level; thus, indicating that 100 μL of ERLs was sufficient to label all antigens captured on the substrate for the 100 ng/mL sample. It is worth noting that analysis of samples with a concentration greater than 100 ng/mL may result in more captured antigens and therefore require a greater ERL volume to fully label all antigen molecules. Importantly, the signal of the negative control samples did not statistically differ among any of the ERL volumes tested. Therefore, based on the parameters used in this optimization study, 200 μL of ERLs were considered optimized and used for subsequent assays.

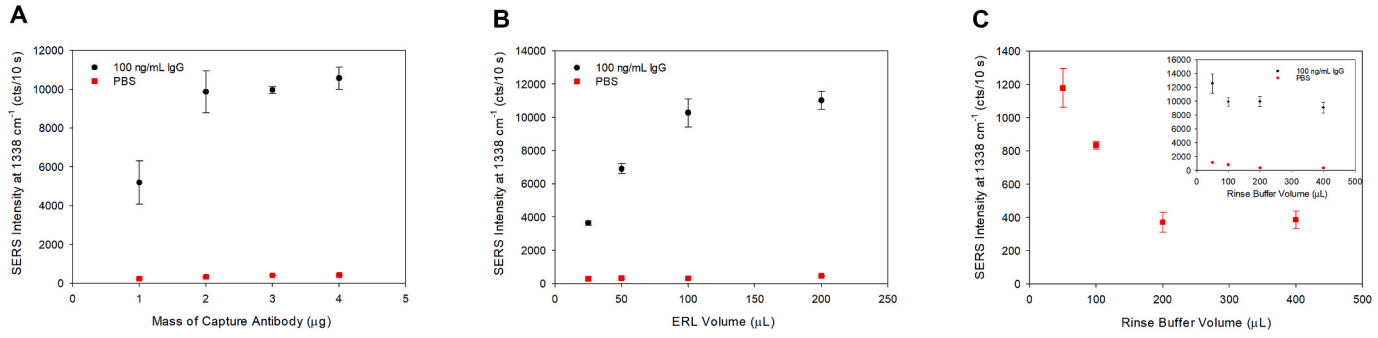

Fig. 4. SERS response of assay optimization parameters: (A) effect of mass of goat ant-mouse IgG capture antibody deposited on the paper substrate, (B) effect of ERL Volume, and (C) effect of rinse buffer volume. A positive control sample (100 ng/mL mouse IgG) and a negative control sample (PBS) were analyzed for each assay condition. Each data point is the average of five measurements, and the error bars represent the standard deviation.

3.4.3. Volume of rinsing buffer

We investigated the effect of rinsing volume in an effort to minimize non-specific binding. In this study, positive (100 ng/mL antigen) and negative (PBS) were analyzed by the vertical flow assay using the optimized mass of capture antibody (2 μg) and volume of ERLs (200 μL). Following the labeling step, different volumes of the rinsing buffer were applied to the sample well and passed through the capture substrate to remove non-specifically bound ERLs. Fig. 4C plots the SERS intensities for the negative control samples as a function of rinse buffer volume. The signal for the negative control sample is a measure of the non-specific binding, and the data show that the negative control signal decreases as the volume of rinse buffer increases from 50 to 200 μL. These data clearly show that excess unbound ERLs remain in the capture substrate filter paper when the rinse volume was less than 200 μL. An increase to 400 μL of PBS rinsing buffer did not lead to a further reduction in the background signal. Fig. 4C (inset) plots the signal collected for the positive control samples as a function of PBS rinsing volume. As is evident, the data show a decrease in the signal for the positive control sample as the rinse volume increases from 50 to 100 μL, which is likely due to the removal of excess unbound ERLs. The positive control signal is independent of rinse volumes between 100 and 400 μL, which suggests that these volumes do not disrupt the specific antibody-antigen interactions. Based on the assessment of these results, we selected 300 μL of rinsing volume for subsequent optimized assays. This volume of rinsing buffer ensures a thorough removal of excess, non-specifically bound ERLs and maintains the maximum analytical signal, while balancing the assay time. Larger volumes require more time for the buffer to pass through the capture substrate, and it is noteworthy that the flow rate decreases as the absorbent pad becomes saturated with liquid.

3.5. Analytical performance – dynamic range, detection limit, reproducibility, sample matrix

The analytical performance of the assay was evaluated using the optimized conditions to generate a calibration curve for the analysis of mouse IgG and establish the dynamic range, detection limit, and reproducibility. Three assays for mouse IgG were performed on three different weeks using three independently prepared suspensions of ERLs and three independently prepared sets of plasmonic paper. A calibration curve was generated for each independent assay to allow for analysis of intra- and inter-assay reproducibility. Concentration-dependent SERS spectra are presented in Fig. 5A for one calibration dataset. As is evident, the SERS intensity increases with a corresponding increase in antigen concentration. The most intense band at 1338 cm^{-1}, due to the symmetric nitro stretch, is plotted as a function of antigen concentration to generate a calibration curve (Fig. 5B). Each data point represents the average signal collected from five different locations across the capture substrate and the error bars represent the standard deviation. The spot-to-spot variation in analytical signal measured 10–20% for most samples, although at low concentrations, e.g., 0.5 ng/mL, where the signal was small, it varied as much as 37%. Calibration curves for two additional independent assays are presented in Figure S2A. Critical analysis of the raw signals to evaluate the inter-assay reveals that the percent relative standard deviations (%RSD) are 10–30% for a given concentration. Closer inspection of the calibration curves shows that each dataset has a similar curve shape, in which the signal increases for sample concentrations between 0 and 100 ng/mL before reaching a maximum signal as the capture substrate becomes saturated at concentrations greater than 100 ng/mL. Each of the three independent assays shows a slightly different maximum signal at saturation. While the dynamic range and overall curve shape, i.e., binding behavior, is similar for each assay, the differences in maximum signal are attributed to differences in the synthesized plasmonic paper substrates responsible for the SERS enhancement. To support this claim, we recently found ~20% variability in SERS signals collected from plasmonic papers [34]. To account for the differences in plasmonic paper enhancement, each calibration curve was normalized with respect to its maximum signal (Figure S2B). After normalization to account for substrate differences the inter-assay variability was significantly reduced to ~10–20%.

The detection limit of the SERS RVF assay was defined as the antigen concentration that produces a signal equal to the blank signal plus three times the standard deviation of the blank measurement. The calibration data presented in Fig. 5B was best fit to a ligand binding model, i.e., saturation curve (Equation (1)) [27,58],

$$y = \frac{B_{max}x}{K_d + x} \quad (1)$$

where B_{max} represents the maximum binding, i.e., maximum signal, and K_d is the antibody-antigen dissociation constant. Based on the best fit of the data, and replicated signals acquired for the blank, the detection limit was 3 ng/mL. Similar evaluation of the two additional independent calibration datasets presented in Figure S2A resulted in detection limits of 8 and 3 ng/mL. This detection limit is equivalent to that obtained for a solution based assay we previously reported using a similar antibody-antigen system, yet this current platform does not suffer from the hook effect [33]. Moreover, a filter based immunoassay using a syringe to facilitate flow rather than a vertical flow-based absorbent pad yielded a detection limit of 1–10 ng/mL for mouse IgG, but required 1 mL of sample and 10 min to complete the assay rather than the 100 μL of sample and ~2 min assay time required for this current format [32]. It is

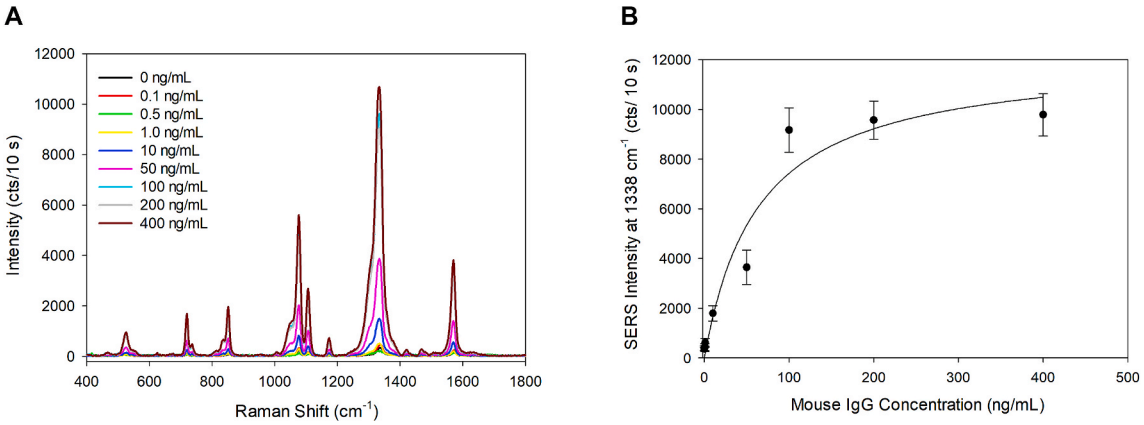

Fig. 5. SERS spectra as a function of antigen concentration acquired using the optimized assay conditions (A). Calibration curve for the optimized SERS assay (B). The SERS intensity of the symmetric NO_2 stretch at 1338 cm^{-1} is plotted as a function of mouse IgG concentration. Each data point is the average of five measurements, and the error bars represent the standard deviation.

worth noting that other vertical flow assays without a plasmonic capture substrate have reported lower detection limits than we present here [25,27,28]; however, those works employed monoclonal antibodies, and it is well-established that the binding affinity of the antibody-antigen governs the detection limit; thus, we can only compare to other studies that used goat anti-mouse IgG polyclonal antibodies as a model system.

In an effort to determine the effect of sample matrix on the assay performance, calibration standard solutions of mouse IgG antigen were prepared in PBS and in 10% rabbit serum. The calibration curves generated with each of these solvents are overlaid in Figure S3. Similar calibration curves are obtained for each of these sample matrices and provide two key findings. First, these results confirm that the assay can capture the antigen protein in the presence of a complex biological matrix. Second, this experiment validates the specificity of the immunoassay given that rabbit serum contains a large concentration of rabbit IgG which is not detected by the anti-mouse IgG capture substrate and ERLs.

3.6. Application of the SERS-RVF to the analysis of mouse serum

Based on these encouraging results, we then applied our SERS-RVF assay to determine the concentration of mouse IgG in mouse serum. IgG is an abundant protein found in serum and has normal concentration range of 5–13 mg/mL in serum collected from healthy mice. Given that the concentration of mouse IgG in normal serum is outside of the limit of linearity for the SERS-RVF assay, the mouse serum was diluted $1{:}10^6$ using PBS as a diluent. We prepared three independent mouse serum samples and the diluted serum samples were analyzed using a newly prepared set of plasmonic paper capture substrates. Concurrently, the capture substrates were used to analyze mouse IgG standards to generate a calibration curve. The IgG concentration in the diluted serum measured 11 ± 3 ng/mL, based on the best fit of the calibration data to the ligand binding curve, which translates to an IgG concentration of 11 ± 3 mg/mL in the original undiluted mouse serum sample. This experimental IgG concentration in normal mouse serum is in the expected range and is consistent with measured values for mouse IgG in normal serum.

4. Conclusions

In this work, we developed a SERS-based RVF assay employing plasmonic paper as the capture substrate. Using mouse IgG as a model antigen, we established a novel strategy to promote a significant signal enhancement for SERS detection by AuNP-embedded filter paper compared to previously utilized paper-based substrates. Our approach takes advantage of the plasmonic coupling between the underlying plasmonic paper capture substrate and the nanoparticle labels, e.g., ERLs, to generate exceedingly large signals for the Raman reporter molecule, e.g., NBT, immobilized on the ERL. Moreover, the vertical flow format enables the capture and concentration of analyte from a small volume sample for rapid detection using capillary action to actively transport the sample through the capture substrate to overcome diffusion limited mass transport [52,53]. Lastly, the vertical flow approach is not complicated by the hook effect for the analysis of highly concentrated samples [13–15]. The ease of use, speed of analysis, low detection limits, and low cost of components suggest this RVF assay is poised to meet the demands of point-of-care diagnostic testing, on-site environmental analysis, and point-of-need biodefense applications.

Credit author statement

Richard Frimpong: Methodology, Validation, Investigation, Writing, Wongi Jang: Methodology, Validation, Investigation, Jun-Hyun Kim: Conceptualization, Methodology, Writing, Supervision, Project administration, Jeremy D. Driskell: Conceptualization, Methodology, Writing, Supervision. Project administration, Funding acquisition

Declaration of competing interest

The authors declare that they have no known competing financial interests or personal relationships that could have appeared to influence the work reported in this paper.

Acknowledgements

This work was supported by in part by the National Science Foundation through the Macromolecular, Supramolecular and Nanochemistry Program, Award # CHE-1807126. Additional funding was provided by the Defense Threat Reduction Agency, Basic Research Award # HDTRA1-13-1-0028.

Appendix A. Supplementary data

Supplementary data to this article can be found online at https://doi.org/10.1016/j.talanta.2020.121739.

References

[1] V. Gubala, L.F. Harris, A.J. Ricco, M.X. Tan, D.E. Williams, Point of care diagnostics: status and future, Anal. Chem. 84 (2) (2012) 487–515.
[2] A. St John, C.P. Price, Existing and emerging technologies for point-of-care testing, Clin. Biochem. Rev. 35 (3) (2014) 155–167.
[3] L. Syedmoradi, M. Daneshpour, M. Alvandipour, F.A. Gomez, H. Hajghassem, K. Omidfar, Point of care testing: the impact of nanotechnology, Biosens. Bioelectron. 87 (2017) 373–387.
[4] G.A. Posthuma-Trumpie, J. Korf, A. van Amerongen, Lateral flow (immuno) assay: its strengths, weaknesses, opportunities and threats. A literature survey, Anal. Bioanal. Chem. 393 (2) (2009) 569–582.
[5] A. Pal, T.K. Dhar, An analytical device for on-site immunoassay. Demonstration of its applicability in semiquantitative detection of aflatoxin B-1 in a batch of samples with ultrahigh sensitivity, Anal. Chem. 76 (1) (2004) 98–104.
[6] G. Rundstrom, A. Jonsson, O. Martensson, I. Mendel-Hartvig, P. Venge, Lateral flow immunoassay using europium (III) chelate microparticles and time-resolved fluorescence for eosinophils and neutrophils in whole blood, Clin. Chem. 53 (2) (2007) 342–348.
[7] S. Choi, E.Y. Choi, D.J. Kim, J.H. Kim, T.S. Kim, S.W. Oh, A rapid, simple measurement of human albumin in whole blood using a fluorescence immunoassay (I), Clin. Chim. Acta 339 (1–2) (2004) 147–156.
[8] S.W. Oh, J.D. Moon, S.Y. Park, H.J. Jang, J.H. Kim, K.B. Nahm, E.Y. Choi, Evaluation of fluorescence hs-CRP immunoassay for point-of-care testing, Clin. Chim. Acta 356 (1–2) (2005) 172–177.
[9] N.V. Zaytseva, R.A. Montagna, E.M. Lee, A.J. Baeumner, Multi-analyte single-membrane biosensor for the serotype-specific detection of Dengue virus, Anal. Bioanal. Chem. 380 (1) (2004) 46–53.
[10] J. Hwang, S. Lee, J. Choo, Application of a SERS-based lateral flow immunoassay strip for the rapid and sensitive detection of staphylococcal enterotoxin B, Nanoscale 8 (22) (2016) 11418–11425.
[11] Z. Rong, R. Xiao, S. Xing, G. Xiong, Z. Yu, L. Wang, X. Jia, K. Wang, Y. Cong, S. Wang, SERS-based lateral flow assay for quantitative detection of C-reactive protein as an early bio-indicator of a radiation-induced inflammatory response in nonhuman primates, Analyst 143 (9) (2018) 2115–2121.
[12] D. Zhang, L. Huang, B. Liu, H. Ni, L. Sun, E. Su, H. Chen, Z. Gu, X. Zhao, Quantitative and ultrasensitive detection of multiplex cardiac biomarkers in lateral flow assay with core-shell SERS nanotags, Biosens. Bioelectron. 106 (2018) 204–211.
[13] S. Dodig, Interferences in quantitative immunochemical methods, Biochem. Med. 19 (1) (2009) 50–62.
[14] X. Liu, Q. Huo, A washing-free and amplification-free one-step homogeneous assay for protein detection using gold nanoparticle probes and dynamic light scattering, J. Immunol. Methods 349 (1–2) (2009) 38–44.
[15] C. Selby, Interference in immunoassay, Ann. Clin. Biochem. 36 (6) (1999) 704–721.
[16] P. Chen, M. Gates-Hollingsworth, S. Pandit, A. Park, D. Montgomery, D. AuCoin, J. Gu, F. Zenhausern, Paper-based vertical flow immunoassay (VFI) for detection of bio-threat pathogens, Talanta 191 (2019) 81–88.
[17] Y. Jiao, C. Du, L. Zong, X. Guo, Y. Han, X. Zhang, L. Li, C. Zhang, Q. Ju, J. Liu, H.-D. Yu, W. Huang, 3D vertical-flow paper-based device for simultaneous detection of multiple cancer biomarkers by fluorescent immunoassay, Sensor. Actuator. B Chem. 306 (2020) 127239.
[18] Y.K. Oh, H.-A. Joung, S. Kim, M.-G. Kim, Vertical flow immunoassay (VFA) biosensor for a rapid one-step immunoassay, Lab Chip 13 (5) (2013) 768–772.
[19] G.M.S. Ross, G.I. Salentijn, M.W.F. Nielen, A critical comparison between flow-through and lateral flow immunoassay formats for visual and smartphone-based multiplex allergen detection, Biosensors 9 (4) (2019) 143.
[20] Z. Cheng, R. Wang, Y. Xing, L. Zhao, J. Choo, F. Yu, SERS-based immunoassay using gold-patterned array chips for rapid and sensitive detection of dual cardiac biomarkers, Analyst 144 (22) (2019) 6533–6540.

[21] D.S. Grubisha, R.J. Lipert, H.-Y. Park, J. Driskell, M.D. Porter, Femtomolar detection of prostate-specific antigen: an immunoassay based on surface-enhanced Raman scattering and immunogold labels, Anal. Chem. 75 (21) (2003) 5936–5943.
[22] N. Guarrotxena, G.C. Bazan, Antibody-functionalized SERS tags with improved sensitivity, Chem. Commun. 47 (31) (2011) 8784–8786.
[23] M.D. Porter, R.J. Lipert, L.M. Siperko, G. Wang, R. Narayanana, SERS as a bioassay platform: fundamentals, design, and applications, Chem. Soc. Rev. 37 (5) (2008) 1001–1011.
[24] B.J. Yun, W.-G. Koh, Highly-sensitive SERS-based immunoassay platform prepared on silver nanoparticle-decorated electrospun polymeric fibers, J. Ind. Eng. Chem. 82 (2020) 341–348.
[25] R. Chen, B. Liu, H. Ni, N. Chang, C. Luan, Q. Ge, J. Dong, X. Zhao, Vertical flow assays based on core–shell SERS nanotags for multiplex prostate cancer biomarker detection, Analyst 144 (13) (2019) 4051–4059.
[26] O.J.R. Clarke, B.L. Goodall, H.P. Hui, N. Vats, C.L. Brosseau, Development of a SERS-based rapid vertical flow assay for point-of-care diagnostics, Anal. Chem. 89 (3) (2017) 1405–1410.
[27] J.H. Granger, A. Skuratovsky, M.D. Porter, Courtney L. Scaife, J.E. Shea, Q. Li, S. Wang, Coupling solid-phase microextractions and surface-enhanced Raman scattering: towards a point-of-need tool for hepatic cancer screening, Anal. Meth. 9 (32) (2017) 4641–4646.
[28] D. Zhang, L. Huang, B. Liu, Q. Ge, J. Dong, X. Zhao, A vertical flow microarray chip based on SERS nanotags for rapid and ultrasensitive quantification of α-fetoprotein and carcinoembryonic antigen, Microchim. Acta 186 (11) (2019) 699.
[29] S.-Y. Chen, A.A. Lazarides, Quantitative amplification of Cy5 SERS in 'warm spots' created by plasmonic coupling in nanoparticle assemblies of controlled structure, J. Phys. Chem. C 113 (28) (2009) 12167–12175.
[30] J.D. Driskell, R.J. Lipert, M.D. Porter, Labeled gold nanoparticles immobilized at smooth metallic substrates: systematic investigation of surface plasmon resonance and surface-enhanced Raman scattering, J. Phys. Chem. B 110 (35) (2006) 17444–17451.
[31] L. Guerrini, F. McKenzie, A.W. Wark, K. Faulds, D. Graham, Tuning the interparticle distance in nanoparticle assemblies in suspension via DNA-triplex formation: correlation between plasmonic and surface-enhanced Raman scattering responses, Chem. Sci. 3 (7) (2012) 2262–2269.
[32] M.A. Penn, D.M. Drake, J.D. Driskell, Accelerated surface-enhanced Raman spectroscopy (SERS)-Based immunoassay on a gold-plated membrane, Anal. Chem. 85 (2013) 8609–8617.
[33] A. Lopez, F. Lovato, S.H. Oh, Y.H. Lai, S. Filbrun, E.A. Driskell, J.D. Driskell, SERS immunoassay based on the capture and concentration of antigen-assembled gold nanoparticles, Talanta 146 (2016) 388–393.
[34] J.A. Lartey, J.P. Harms, R. Frimpong, C.C. Mulligan, J.D. Driskell, J.-H. Kim, Sandwiching analytes with structurally diverse plasmonic nanoparticles on paper substrates for surface enhanced Raman spectroscopy, RSC Adv. 9 (2019) 32535–32543.
[35] J. Turkevich, P.C. Stevenson, J. Hillier, A study of the nucleation and growth processes in the synthesis of colloidal gold, Discuss. Faraday Soc. 11 (1951) 55–75, 0.
[36] M. Wuithschick, A. Birnbaum, S. Witte, M. Sztucki, U. Vainio, N. Pinna, K. Rademann, F. Emmerling, R. Kraehnert, J. Polte, Turkevich in new robes: key questions answered for the most common gold nanoparticle synthesis, ACS Nano 9 (7) (2015) 7052–7071.
[37] S. Hong, X. Li, Optimal size of gold nanoparticles for surface-enhanced Raman spectroscopy under different conditions, J. Nanomater. 2013 (2013) 790323.
[38] J.K. Yoon, K. Kim, K.S. Shin, Raman scattering of 4-aminobenzenethiol sandwiched between Au nanoparticles and a macroscopically smooth Au substrate: effect of size of Au nanoparticles, J. Phys. Chem. C 113 (2009) 1769–1774.
[39] J.-H. Kim, K.M. Twaddle, L.M. Cermak, W. Jang, J. Yun, H. Byun, Photothermal heating property of gold nanoparticle loaded substrates and their SERS response, Colloids Surf., A 498 (2016) 20–29.
[40] Y.H. Ngo, D. Li, G.P. Simon, G. Garnier, Gold nanoparticle–paper as a three-dimensional surface enhanced Raman scattering substrate, Langmuir 28 (23) (2012) 8782–8790.
[41] Y.H. Ngo, D. Li, G.P. Simon, G. Garnier, Effect of cationic polyacrylamide dissolution on the adsorption state of gold nanoparticles on paper and their Surface Enhanced Raman Scattering properties, Colloids Surf., A 420 (2013) 46–52.
[42] G. Wang, H.-Y. Park, R.J. Lipert, M.D. Porter, Mixed monolayers on gold nanoparticle labels for multiplexed surface-enhanced Raman scattering based immunoassays, Anal. Chem. 81 (23) (2009) 9643–9650.
[43] J.L. Abell, J.M. Garren, Y. Zhao, Dynamic rastering surface-enhanced Raman scattering (SERS) measurements on silver nanorod substrates, Appl. Spectrosc. 65 (7) (2011) 734–740.
[44] H. de Puig, I. Bosch, M. Carré-Camps, K. Hamad-Schifferli, Effect of the protein corona on antibody–antigen binding in nanoparticle sandwich immunoassays, Bioconjugate Chem. 28 (1) (2017) 230–238.
[45] S.L. Filbrun, J.D. Driskell, A fluorescence-based method to directly quantify antibodies immobilized on gold nanoparticles, Analyst 141 (12) (2016) 3851–3857.
[46] G. Ruiz, N. Ryan, K. Rutschke, O. Awotunde, J.D. Driskell, Antibodies irreversibly adsorb to gold nanoparticles and resist displacement by common blood proteins, Langmuir 35 (32) (2019) 10601–10609.
[47] A. Wang, K. Vangala, T. Vo, D. Zhang, N.C. Fitzkee, A three-step model for protein–gold nanoparticle adsorption, J. Phys. Chem. C 118 (15) (2014) 8134–8142.
[48] O. Awotunde, S. Okyem, R. Chikoti, J.D. Driskell, Role of free thiol on protein adsorption to gold nanoparticles, Langmuir 36 (31) (2020) 9241–9249.
[49] K. Siriwardana, A. Wang, K. Vangala, N. Fitzkee, D. Zhang, Probing the effects of cysteine residues on protein adsorption onto gold nanoparticles using wild-type and mutated GB3 proteins, Langmuir 29 (35) (2013) 10990–10996.
[50] J.D. Driskell, C.G. Larrick, C. Trunell, Effect of hydration on plasmonic coupling of bioconjugated gold nanoparticles immobilized on a gold film probed by surface-enhanced Raman spectroscopy, Langmuir 30 (22) (2014) 6309–6313.
[51] H.K. Lee, Y.H. Lee, C.S.L. Koh, G.C. Phan-Quang, X. Han, C.L. Lay, H.Y.F. Sim, Y.-C. Kao, Q. An, X.Y. Ling, Designing surface-enhanced Raman scattering (SERS) platforms beyond hotspot engineering: emerging opportunities in analyte manipulations and hybrid materials, Chem. Soc. Rev. 48 (2019) 731–756.
[52] D.G. Myszka, T.A. Morton, M.L. Doyle, I.M. Chaiken, Kinetic analysis of a protein antigen-antibody interaction limited by mass transport on an optical biosensor, Biophys. Chem. 64 (1) (1997) 127–137.
[53] H. Nygren, M. Werthen, M. Stenberg, Kinetics of antibody binding to solid-phase-immobilised antigen: effect of diffusion rate limitation and steric interaction, J. Immunol. Methods 101 (1) (1987) 63–71.
[54] M. Al-Tamimi, W. Shen, R. Zeineddine, H. Tran, G. Garnier, Validation of paper-based assay for rapid blood typing, Anal. Chem. 84 (3) (2012) 1661–1668.
[55] J. Wang, B. Yiu, J. Obermeyer, C.D.M. Filipe, J.D. Brennan, R. Pelton, Effects of temperature and relative humidity on the stability of paper-immobilized antibodies, Biomacromolecules 13 (2) (2012) 559–564.
[56] I.R. Lewis, N.W. Daniel, P.R. Griffiths, Interpretation of Raman spectra of nitro-containing explosive materials. Part I: group frequency and structural class membership, Appl. Spectrosc. 51 (12) (1997) 1854–1867.
[57] D.S. Moore, S.D. McGrane, Comparative infrared and Raman spectroscopy of energetic polymers, J. Mol. Struct. 661–662 (2003) 561–566.
[58] D. Wild, C. Sheehan, Standardization and calibration, in: D. Wild (Ed.), The Immunoassay Handbook: Theory and Applications of Ligand Binding, ELISA and Related Techniques 2013.